Convective heat and mass transfer modeling under crystal growth by vertical Bridgman method

IOP Conf. Series: Journal of Physics: Conf. Series **1479** (2020) 012029 doi:10.1088/1742-6596/1479/1/012029

Convective heat and mass transfer modeling under crystal growth by vertical Bridgman method

A I Fedyushkin[1], **N G Burago**[1], **A A Puntus**[2]

[1]Ishlinsky Institute for Problems in Mechanics of RAS, Moscow, Russia
[2]Moscow Aviation Institute (National Research University), Moscow, Russia

E-mail: fai@ipmnet.ru

Abstract. This paper presents the results of numerical modeling by the finite element method (FEM) of convective heat and mass transfer during the growth of single crystals by the vertical Bridgman method with a submerged heater. Numerical calculations were performed using the implicit matrixless finite element method based on the iterative process of conjugate gradients and significantly reducing the requirements for RAM and computer speed. The effects of gravity, rotation, crystallization rate and vibration on heat and mass transfer in the melt, the geometry of the crystallization front, and the thickness of the boundary layers were studied. It is shown that the above effects can be effectively used to control the distribution of impurities in crystals grown by the vertical Bridgman method.

1. Introduction

The technologies for growing perfect single crystals are faced with the task of improving their uniformity and increasing productivity that is, increasing the crystal growth rate [1-3]. To solve these problems, it is necessary to organize the convective mixing of the melt in such a way that the following conditions are met: 1) uniform and quick removal of heat from the growing crystal, 2) maintaining a flat form of the crystallization front and 3) uniform impurity distribution along the radius of the crystal. The heat and mass transfer during crystal growth can be controlled using the optimal selection of geometry, thermal parameters, growth rate, as well as various physical and mechanical controlled influences (rotation, vibration, magnetic and gravitational fields) [3-8]. The authors of [3] give an overview of the results of crystal growth under rotational and vibrational influences on the melt flow. In [4-8], the results of mathematical modeling of the effects of gravity, rotational and vibrational effects on heat and mass transfer during crystal growth are presented. Reviews of the results of mathematical modeling of heat and mass transfer during crystal growth and the prospects for the development of these works are given in [9-10]. In [11], heat and mass transfer was simulated numerically for the vertical Bridgman method with submerged heater. The submerged heater separates the region of melt near growing crystal and allows control of convective mixing of dopant near the crystallization front. A review of Bridgman method with submerged heater is presented in [12]. In [13] the effect of submerged heater rotation on the shape of crystallization front of $NaNO_3$ crystal was studied numerically and experimentally.

This paper presents the results of finite element modeling of convective heat and mass transfer in single crystal growth by vertical Bridgman method with submerged heater. The effects of gravity, rotation, crystallization rate and vibration on heat and mass transfer in melt, on thickness of boundary

layers and on distribution of dopant in crystals are studied. The details of numerical methods and models used in this work can be found in [14-15].

2. Mathematical model

The axisymmetric unsteady melt flow is described by the Navier equations for an incompressible fluid in the Boussinesq approximation. The incompressibility condition, the equations of motion in projections onto the radial, circumferential and axial directions, the heat equation and the convection-diffusion equation of the impurity are written below:

$$\frac{\partial u}{\partial r}+\frac{u}{r}+\frac{\partial w}{\partial z}=0 \tag{1}$$

$$\rho_0\frac{du}{dt}-\frac{\rho_0 v^2}{r}=-\frac{\partial p}{\partial r}+\frac{1}{r}\frac{\partial}{\partial r}\left(r\mu\frac{\partial u}{\partial r}\right)+\frac{\partial}{\partial z}\left(\mu\frac{\partial w}{\partial z}\right)-\mu\frac{u}{r^2} \tag{2}$$

$$\rho_0\frac{dv}{dt}+\frac{\rho_0 uv}{r}=\frac{1}{r}\left(r\mu\frac{\partial v}{\partial r}\right)+\frac{\partial}{\partial z}\left(\mu\frac{\partial v}{\partial z}\right)-\mu\frac{v}{r^2} \tag{3}$$

$$\rho_0\frac{dw}{dt}=-\frac{\partial p}{\partial z}+\frac{1}{r}\frac{\partial}{\partial r}\left(r\mu\frac{\partial w}{\partial r}\right)+\frac{\partial}{\partial z}\left(\mu\frac{\partial w}{\partial z}\right)-\rho_0 g\beta(T-T_0) \tag{4}$$

$$c_V\frac{dT}{dt}=\frac{1}{r}\frac{\partial}{\partial r}\left(k_T r\frac{\partial T}{\partial r}\right)+\frac{\partial}{\partial z}\left(k_T\frac{\partial T}{\partial z}\right) \tag{5}$$

$$\frac{dC}{dt}=\frac{1}{r}\frac{\partial}{\partial r}\left(k_C r\frac{\partial C}{\partial r}\right)+\frac{\partial}{\partial z}\left(k_C\frac{\partial C}{\partial z}\right) \tag{6}$$

where $d/dt=\partial/\partial t+u\partial/\partial r+w\partial/\partial z$ is material time derivative, u,v,w are radial, circumferential and axial velocities, μ,k_T,k_C are dynamic viscosity, heat conduction and diffusion coefficients, β is the buoyancy coefficient, T_0 is a reference temperature, ρ_0 is a reference density, g is the gravity acceleration along z.

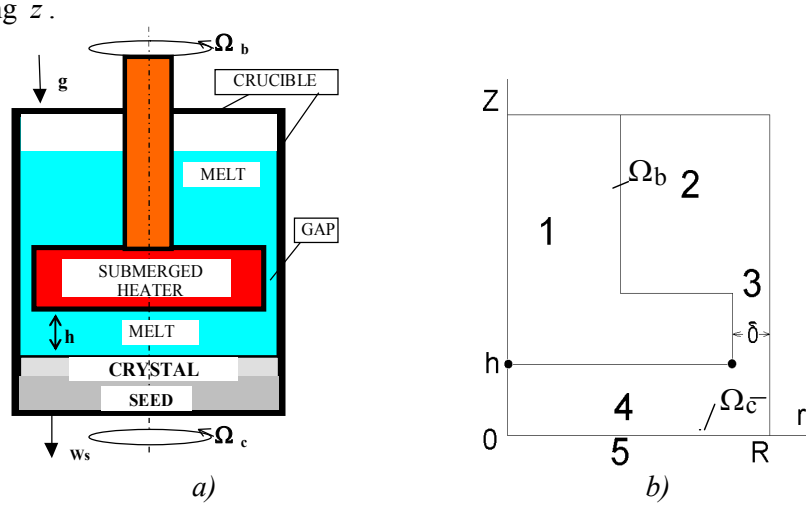

a) *b)*

Figure 1. Schematic of Bridgman method with submerged heater (a) and solution domain (b).

The solution domain is shown in Figure 1, where $R=3.36cm$ is the radius of crucible, $=\delta 0.1cm$ is the size of the gap $h=0.8cm$, S_{SH} is the region of the submerged heater. The crystallization front (5) is considered flat and the crystal growth rate is constant, is the melting temperature of germanium, is the concentration of gallium impurity. On solid walls, adhesion conditions is specified, Ω_{CR} is

crucible rotation speed (including crystal and vertical crucible walls), Ω_b is the rotation speed of the submerged heater. The boundary conditions are accepted as:

$$r=0,\ 0\le z\le H\ :\ u=0,\ v=0,\ \partial w/\partial r=0,\ \partial T/\partial r=0,\ \partial C/\partial r=0 \quad (7)$$

$$0\le r\le R,\ z=0\ :\ u=0,\ v=0,\ w=-W_s,\ T=T_m,\ k_C\partial C/\partial z=W_sC(1-k_0) \quad (8)$$

$$r=R,\ 0\le z\le h\ :\ u=0,\ v=0,\ w=0,\ \partial T/\partial r=0,\ \partial C/\partial r=0 \quad (9)$$

$$r=R,\ h<z\le H\ :\ u=0,\ v=0,\ w=0,\ T=T_{CR}(z),\ \partial C/\partial r=0 \quad (10)$$

$$(r,z)\in S_{SH}:\ u=0,\ v=0,\ w=0,\ T=T_{SH}(r,z,t),\ \partial C/\partial n=0 \quad (11)$$

$$0\le r\le R,\ z=H\ :\ u=0,\ \partial v/\partial z=0,\ \partial w/\partial z=0,\ T=T_Z,\ C=C_{02} \quad (12)$$

Initial conditions are

$$t=0,\ 0\le r\le R,\ 0\le z\le h\ :\ u=0,\ v=0,\ w=-W_s,\ T=T_m,\ C=C_{01} \quad (13)$$

$$t=0,\ 0\le r\le R,\ h<z\le H\ :\ u=0,\ v=0,\ w=-W_s,\ T=T_m,\ C=C_{02} \quad (14)$$

At the crystallization front, the condition of mass transfer of the third kind (8) is set taking into account the crystallization rate W_s and with the equilibrium extrusion coefficient of impurity k_0. Vibrations were specified as a harmonic function of time for movement or speed on a submerged vibrator. The task is characterized by the following similarity numbers: Reynolds number associated with the crystal growth rate $Re_s=W_SR/\nu$; vibrational Reynolds number $Re_{vibr}=A\omega R/\nu$, where A is the amplitude, $\omega=2\pi f$ is circular frequency of translator's vibrations; Prandtl number $Pr=\mu c_p/k_T$; Grashof number $Gr=g\beta\Delta TR^3\rho_0^2/\mu^2$ (or Rayleigh number $Ra=Gr\cdot Pr$), where ΔT is the temperature range.

3. Numerical method

Initial boundary value problem for Navier-Stokes equations (1) - (14) is solved by implicit matrix-free scheme using piecewise linear approximation of the solution on triangular finite elements (detailed description is given in [14]). For example consider typical convection-diffusion initial boundary value problem for unknown function $A(x,t)$:

$$t\ge 0,\ x\in V:\ \frac{\partial A}{\partial t}+u\cdot\nabla A=\nabla\cdot(k\nabla A)+F \quad (15)$$

$$t=0,\ x\in V:\ \mathrm{A}=\mathrm{A}^0(x)$$

$$t\ge 0,\ x\in S_A:\ A(x,t)=A_*(x,t)$$

$$t\ge 0,\ x\in S\setminus S_A:\ k\nabla A=P_*(x,t)$$

where values with stars are predefined and $S=\partial V$, $S_A\subset S$, the following variational implicit scheme was used (n is time layer number, n=0,1,2…):

$$\int_V\left(\frac{A^{n+1}-A^n}{\Delta t^n}+u^n\cdot\nabla A^{n+1}\right)\left(\delta A+\Delta t^n u^n\cdot\nabla\delta A\right)dV+\int_V\tilde{k}^n\nabla A^{n+1}\cdot\nabla\delta A\,dV=\int_V F^{n+1}\cdot\delta\mathrm{A}\,dV+\int_{S\setminus S_A}P_*^{n+1}\cdot\delta A\,dS \quad (16)$$

$$t=t^n,\ x\in V:\ \mathrm{A}=\mathrm{A}^n(x)$$

$$t\ge 0,\ x\in S_A:\ A^{n+1}(x,t)=A_*^{n+1}(x,t)$$

Coefficient $\tilde{k}^n \geq 0$ represents corrected viscosity coefficient. It is decreased according to exponential fitting technique [16] (in simplest manner): $\tilde{k}^n = k^2 / (k + u^n \cdot u^n \Delta t^n)$. In order to account incompressibility the penalty functions method is used: pressure is calculated by formula $p = -\lambda \rho_0 (max\{|u|\})^2 (\nabla \cdot u) \Delta t$, where u is the velocity, $\lambda \approx 10$ is dimensionless penalty coefficient, Δt is a time step. Formally, implicit scheme is unconditionally stable. But in order to provide required accuracy of the unsteady solution time step is restricted by usual Courant condition: $\Delta t^n = min(|\Delta x| / |u|)$. At each time step the algebraic system of equations was solved iteratively by matrix-free conjugate gradient method. The implementation requires $4N$ real numbers of operative memory (N is a number of unknown nodal values $\{\{A_i^{n+1}\}_{i=1}^N\}$) and the machine precision of solution is reached after $N^{1/2}$ iterations. To decrease the condition number of algebraic problem the diagonal approximation of the equation matrix was used as preconditioner (scaling of unknowns). The calculation of the residuals of the algebraic equations at each iteration exactly coincides with the calculation of each time step in explicit two-layer finite-element (or finite difference) schemes. So the amount of computations required for finding the solution is proportional to $N^{3/2}$. Detailed description of algorithm is given in [15].

The characteristics of the time-averaged vibrational flows, for example, of a certain value φ during the solution, were determined by the formula:

$$\varphi_{average} = \frac{1}{t} \int_0^t \varphi dt .$$

An additional restriction on the time step to ensure accuracy was determined by the frequency of vibrations. The time step was chosen so that for each period of vibrations of the vibrator we used from 50 to 400 time steps. The results for averaged vibrational flows correspond to times when the averaged flow becomes quasi-stationary.

4. The effect of rotation on the distribution of impurities in a crystal

When single crystals are grown by the vertical Bridgman method, crucible rotation is used to provide symmetry the temperature and impurity distribution [4,7]. Figure 2 shows the isolines of the stream function for two cases: without rotation (Figure 2a) and with rotation (Figure 2b) of the submerged heater at a speed $\Omega_b = 0.3117 rps$. It is seen that the rotation of the submerged heater significantly affects the flow of the germanium melt.

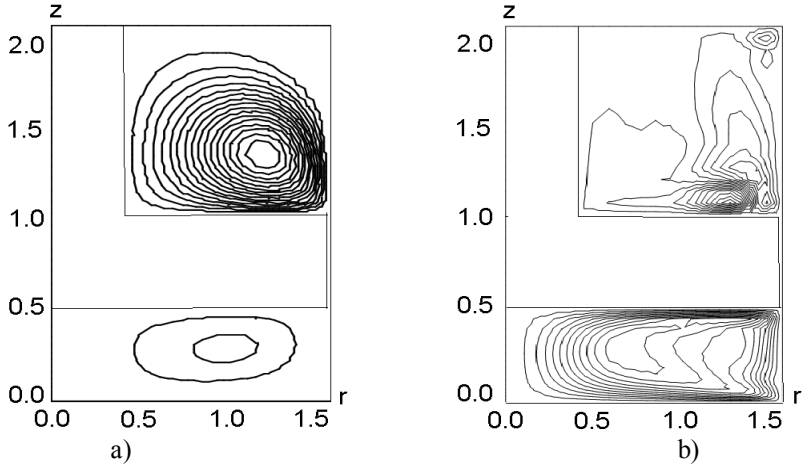

Figure 2. Isolines of flow function a) without rotation and b) with rotation of crucible at a speed $\Omega_b = 0.3117 rps$.

Effect of rotation of crucible and submerged heater on distribution of dopant in the crystal is illustrated by isolines of dopant in Figures 3-4.

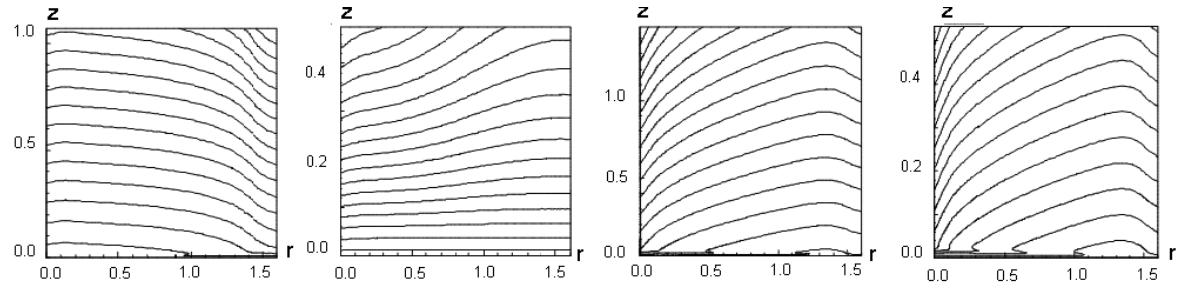

a) b) c) d)

Figure 3. Dopant distribution in the crystal. Without rotation: (a) – terrestrial, (b) – microgravity. With rotation of heater ($\Omega_b = 0.05 rps$): (c) – terrestrial, (d) – microgravity conditions.

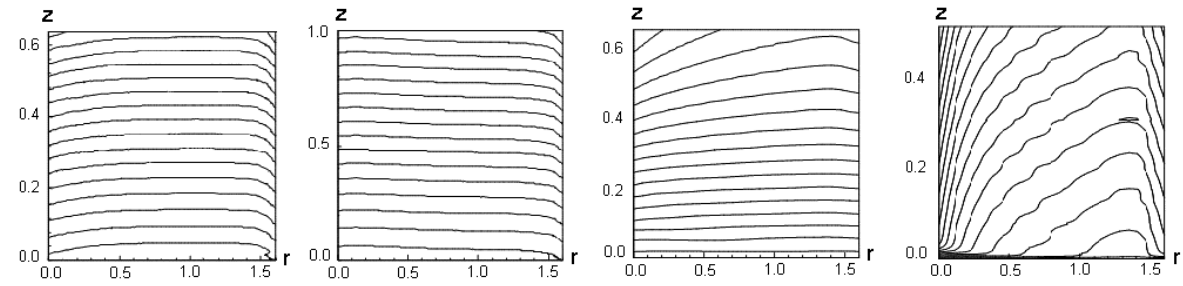

a) b) c) d)

Figure 4. Dopant distribution in the crystal. With rotation of heater and crucible: (a) - $\Omega_b = 0.05 rps$ and $\Omega_b = 0.3117 rps$; (b) - $\Omega_b = 0.05 rps$ and $\Omega_b = 0.3117 rps$. With oscillating rotation of the heater with a frequency of 0.68Hz for two points in time: (c) - t=579 sec and (d) – 816 sec.

The simulation results showed that under terrestrial conditions, the most uniform distribution of impurities in the crystal is obtained by counter rotating the crucible and the submerged heater (Figure 4b).

The effect of harmonic oscillatory rotation of a submerged heater was calculated with a frequency of 0.68Hz. This effect is expressed in the appearance of additional wave-like inhomogeneities in the distribution of impurities in the melt and, as a consequence, in the crystal (Figure 4d).

5. The effect of crystallization rate on the distribution of impurities

The influence of gravity and directed crystallization rate on the distribution of impurities in the melt for vertical Bridgman method with submerged heater was first studied in works [11-13] by the finite difference method. We repeated these calculations by the finite element method (see Figure 5) and obtained excellent agreement with the mentioned results. The results in Figures. 6-7 show the effect of gravity acceleration and crystal growth rate on the distribution of gallium (Ga) in a germanium crystal (Ge) for three cases of growth rate: $W_s = 0.36 rps$, $W_s = 1.8 rps$, $W_s = 3.6 rps$ and two cases of gravity acceleration $g = g_0 = 9.8 m / \sec^2$ and $g = 0.001 g_0$.

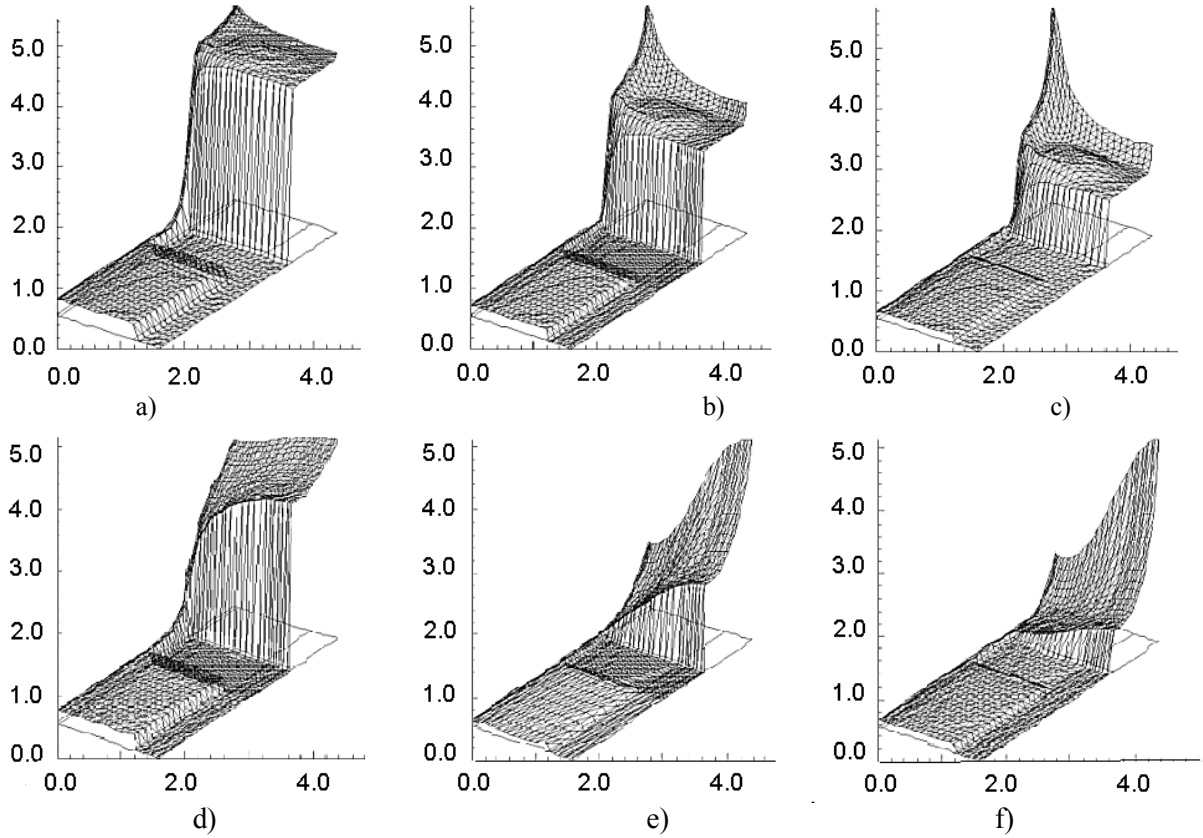

Figure 5. Finite element results for concentration of Ga in the melt Ge (in concord with original [11-13]): upper row for terrestrial gravity $g = g_0$, lower row for microgravity $g = 0.001 g_0$. Growth rate: $W_s = 0.36 cm/h$ for (a) and (d), $W_s = 1.8 cm/h$ for (b) and (e), $W_s = 3.6 cm/h$ for (c) and (f).

Additionally, for each of the presented variants, impurity distributions in crystals were obtained (Figures 6-9). In the mathematical model, it was assumed that the velocity of the planar crystallization front remains constant during a single crystal growth process. The distribution of the impurity in the crystal is calculated by using the obtained history of the impurity at the crystallization front taking into account the crystallization rate W_s and with the equilibrium extrusion coefficient of impurity $k_0 = 0.087$.

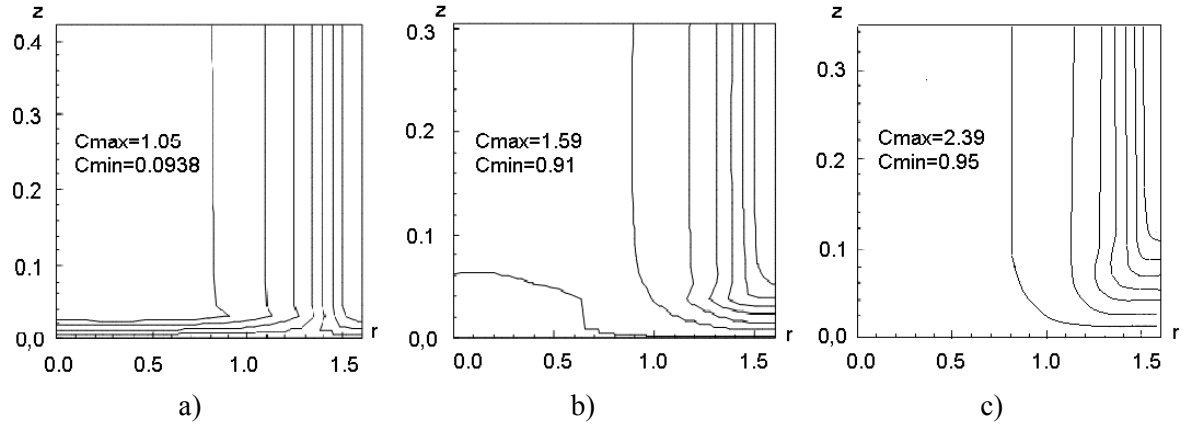

Figure 6. Isolines of concentration of Ga in the melt Ge in terrestrial conditions ($g = g_o$) for various growth rate: $W_s = 0.36 cm/h$ – (a), $1.8 cm/h$ – (b), $3.6 cm/h$ – (c).

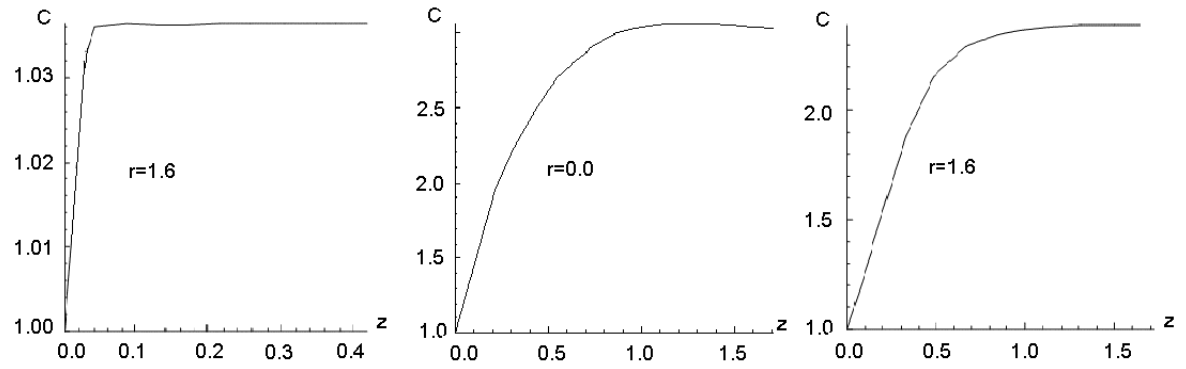

a) b) c)

Figure 7. Distribution of concentration Ga in the crystal Ge along lines r=*const* for various growth rate: $W_s = 0.36cm/h$ – (a), $1.8cm/h$ – (b), $3.6cm/h$ – (c).

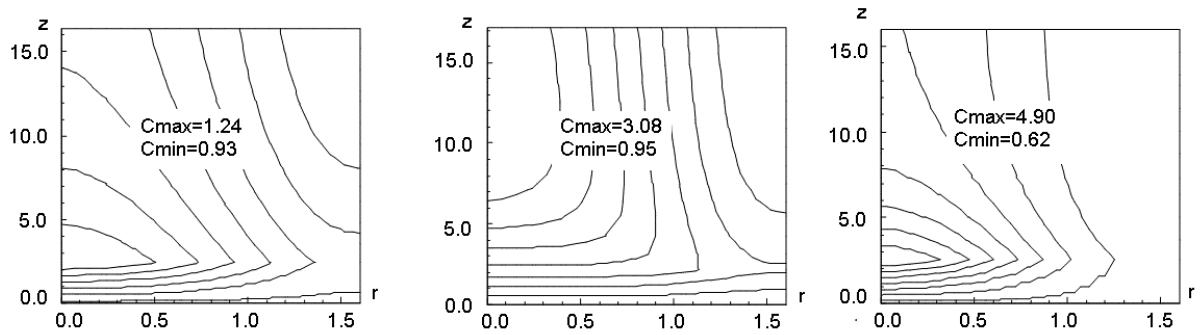

a) b) c)

Figure 8. Isolines of concentration of Ga in the melt Ge in space conditions ($g = 0.001g_o$) for various growth rate: $W_s = 0.36cm/h$ – (a), $1.8cm/h$ – (b), $3.6cm/h$ – (c).

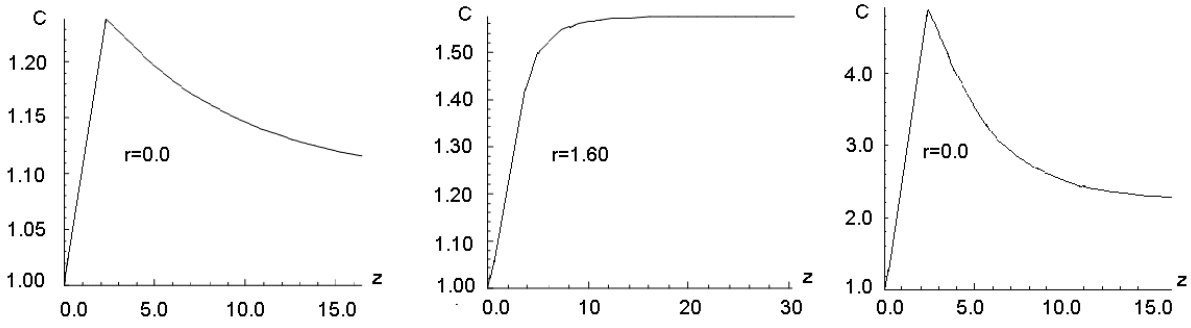

a) b) c)

Figure 9. Distribution of concentration of Ga in the melt Ge in microgravity conditions ($g = 0.001g_o$) for various growth rate: $W_s = 0.36cm/h$ – (a), $1.8cm/h$ – (b), $3.6cm/h$ – (c).

The simulation results showed that the nature of the distribution of the impurity under terrestrial conditions and during microgravity is significantly different, and the most uniform distribution of the impurity in the crystal is obtained at a crystallization rate of $W_s = 1.8cm/h$.

6. Effect of vibrations

Vibrations were set in the form of a harmonic function of time for speed at boundary of crucible or submerged heater (used as vibrators) in accordance with the law: $z = A\cos(2\pi ft)$ with frequency f and small amplitude A. The crystal growth rate was constant $W_s = 0.3cm/h$. The vibration amplitudes were set in the range from 0 to 400 μm, and the frequencies were in the range from 0 to 100 Hz. Figure 10a shows isotherms in the melt (Pr = 5.43) (without vibrations in the right parts of the figures, with vibrations in the left parts ($Re_{vibr} = 200$). The isolines of the stream function in the absence of vibrations of the submerged vibrator (Figure 10b) and with vibrations (Figure 10c).

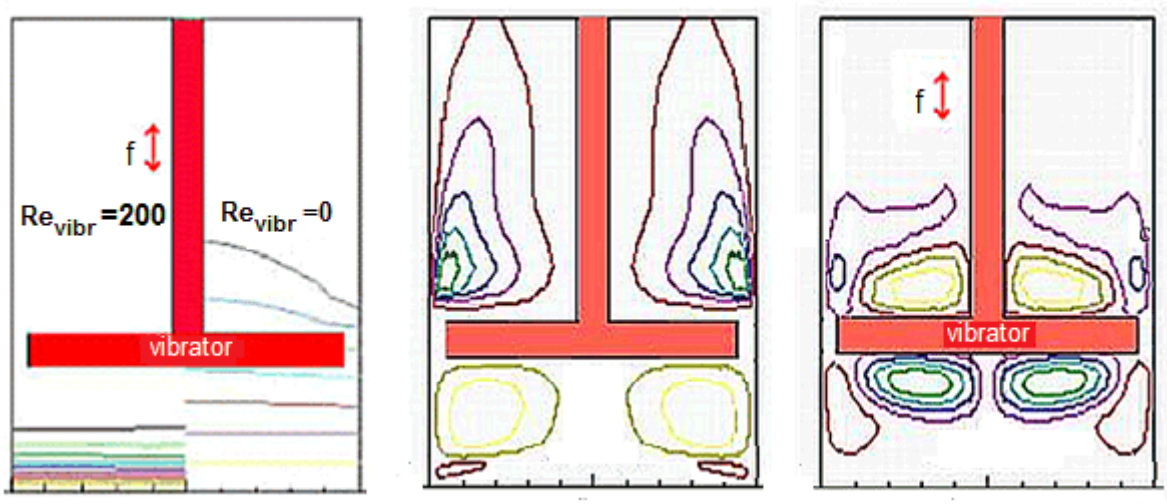

а) б) в)

Figure 10. Bridgman method with submerged vibrator $NaNO_3$: a) isotherms in the melt without vibrations (right part) and with vibration (left part); Isolines of stream function: b) without vibrations (f=0); c) and with vibrations (A = 0.1mm, f = 30Hz).

7. Conclusion

The simulation results showed that rotations in terrestrial and microgravity conditions can homogenize the distribution of the impurity in the crystal. This can be a way to control the distribution of the impurity in the crystal. Rotations under zero gravity conditions can be a necessary alternative to natural convection and intensification of heat removal from a crystal. For optimal distribution of impurities in the crystal, the rotational speeds should be a function of time. Accelerated slow rotation of the submerged heater is most effective for mixing impurities in the melt. Under terrestrial conditions, the most uniform distribution of impurities in the crystal is obtained by counter-rotation of the crucible and the submerged heater. The most uniform distribution of impurities in the crystal is obtained at a crystallization rate of $W_s = 1.8cm/h$. A decrease in the thicknesses of the temperature boundary layers under vibration exposure is shown. The results of numerical simulations showed that it is possible to obtain a flatter crystallization front by vibrational action, which is important when growing single crystals. Rotations along with vibration exposure can be a simple means of control when growing single crystals by the vertical Bridgman method.

References

[1] *Crystal Growth Technology*. 2003 Eds Hans J. Scheel & Tsuguo Fukuda. (Chichester: John Wiley & Sons).
[2] Elwell D and Scheel H J 1975 *Crystal growth from high-temperature solutions* (London, New York, San Francisco: Academic press).

[3] Capper P and Zharikov E 2015 Oscillatory-Driven Fluid Flow Control during Crystal Growth from the Melt. *Handbook of Crystal Growth: Bulk Crystal Growth: Second Edition*. vol. 2 ed P.Rudolph (Amsterdam: Elsevier) p 950-993.

[4] Fedyushkin A 2005 The gravitation, rotation and vibration - controlling factors of the convection and heat–mass transfer. *Proc. Int. Conf. 4th ICCHMT (Paris, France)* p 948-951.

[5] Fedyushkin A Bourago N Polezhaev V and Zharikov E 2005 The influence of vibration on hydrodynamics and heat-mass transfer during crystal growth. *J Crystal Growth* 275(1-2) e1557-63.

[6] Bourago N G Fedyushkin A I and Polezhaev V I 1999. Dopant distribution in crystals grown by the submerged heater method under steady and oscillatory rotation. *Adv Space Res*. 24(10) p 1245-50

[7] Fedyushkin A I Burago N G and Puntus A A 2019 Effect of rotation on impurity distribution in crystal growth by Bridgman method. *Journal of Physics: Conference Series*. 1359 012045. doi:10.1088/1742-6596/1359/1/0120451

[8] Fedyushkin A I and Bourago N G 2001 Influence of vibrations on boundary layers in Bridgman crystal growth. *Proc. 2nd Pan-Pacific Basin Workshop on Microgravity Sciences (Pasadena, USA)* Paper CG-1073. p 1-7

[9] Kakimoto K. and Gao B. Fluid Dynamics 2015 Modeling and Analysis. *Handbook of Crystal Growth: Bulk Crystal Growth: Second Edition*. vol**.** 2, ed P.Rudolph (Amsterdam: Elsevier) p 845-870.

[10] Derby J J and Yeckel A 2015 Heat Transfer Analysis and Design for Bulk Crystal Growth: Perspectives on the Bridgman Method. *Handbook of Crystal Growth Bulk Crystal Growth Second Edition*. vol 2 ed P.Rudolph (Amsterdam: Elsevier) p 793-843

[11] Meyer S and Ostrogorsky A G 1997 Forced convection in vertical Bridgman configuration with the submerged heater. *J. Crystal Growth* 171(3-4) p 566-576.

[12] Jurisch M Eichler S and Bruder M 2015 Vertical Bridgman Growth of Binary Compound Semiconductors. *Handbook of Crystal Growth: Bulk Crystal Growth: Second Edition*. Vol 2 ed P.Rudolph (Amsterdam: Elsevier) p 331-372.

[13] Ostrogorsky A G Riabov V and Dropka N 2018 Interface control by rotating submerged heater/baffle in vertical Bridgman configuration. *J of Crystal Growth* 498 p 269-276.

[14] Burago N G Nikitin I S and Yakushev V L 2016 Hybrid numerical method for unsteady problems of continuum mechanics using arbitrary moving adaptive overlap grids. *Computational Mathematics and Mathematical Physics* 56(6) p 1065–74.

[15] Burago N G and Nikitin I S 2018 Matrix-Free Conjugate Gradient Implementation of Implicit Schemes *Computational Mathematics and Mathematical Physics* 58(8) p 1247-58.

[16] Doolan E P Miller J J H and Schilders W H A 1980 *Uniform Numerical Methods for Problems with Initial and Boundary Layers.* (Dublin: Boole)